ARMY RESEARCH LABORATORY

A Study of Projectile Response to Ballistics Environment

by Stephen E. Ray, Michael J. Nusca, and James F. Newill

ARL-TR-3672 **November 2005**

NOTICES

Disclaimers

The findings in this report are not to be construed as an official Department of the Army position unless so designated by other authorized documents.

Citation of manufacturer's or trade names does not constitute an official endorsement or approval of the use thereof.

Destroy this report when it is no longer needed. Do not return it to the originator.

Army Research Laboratory
Aberdeen Proving Ground, MD 21005-5066

ARL-TR-3672 **November 2005**

A Study of Projectile Response to Ballistics Environment

Stephen E. Ray
U.S. Army High Performance Computing Research Center

Michael J. Nusca and James F. Newill
Weapons and Materials Research Directorate, ARL

REPORT DOCUMENTATION PAGE	Form Approved OMB No. 0704-0188

1. REPORT DATE *(DD-MM-YYYY)*	2. REPORT TYPE	3. DATES COVERED (From - To)
November 2005	Final	September 2004–May 2005

4. TITLE AND SUBTITLE
A Study of Projectile Response to Ballistics Environment

5a. CONTRACT NUMBER
DAAD19-03-D-001

5b. GRANT NUMBER

5c. PROGRAM ELEMENT NUMBER

6. AUTHOR(S)
Stephen E. Ray,* Michael J. Nusca, and James F. Newill

5d. PROJECT NUMBER
622618H8000

5e. TASK NUMBER

5f. WORK UNIT NUMBER

7. PERFORMING ORGANIZATION NAME(S) AND ADDRESS(ES)
U.S. Army Research Laboratory
ATTN: AMSRD-ARL-WM-BD
Aberdeen Proving Ground, MD 21005-5066

8. PERFORMING ORGANIZATION REPORT NUMBER
ARL-TR-3672

9. SPONSORING/MONITORING AGENCY NAME(S) AND ADDRESS(ES)

10. SPONSOR/MONITOR'S ACRONYM(S)

11. SPONSOR/MONITOR'S REPORT NUMBER(S)

12. DISTRIBUTION/AVAILABILITY STATEMENT
Approved for public release; distribution is unlimited.

13. SUPPLEMENTARY NOTES
*U.S. Army High Performance Computing Research Center, Minneapolis, MN

14. ABSTRACT
The U.S. Army Research Laboratory's interior ballistics code, ARL-NGEN3, is a state-of-the-art modeling tool providing interior ballistics predictions and flowfield simulations of the ignition, flamespreading, and combustion of solid-propellant charges used to launch projectiles from guns. Modern solid mechanics codes such as DYNA3D and EPIC can complement the ARL-NGEN3 code by providing a capability to predict the mechanical response of the projectile to the unsteady, high-pressure environment within the gun chamber. This report presents results from an ongoing effort to couple the ARL-NGEN3 code to these solid mechanics codes. The test problem involves a notional gun ammunition concept in which the projectile afterbody "telescopes" or intrudes significantly into the gun chamber that houses the solid propellant charge. Results from the ARL-NGEN3 simulation are shown, and they indicate that large pressure waves move radially and, more significantly, axially through the combustion chamber during propellant ignition. Results from EPIC and DYNA simulations, which utilize the ARL-NGEN3 pressure data and predict material response, are compared; good agreement between the codes is demonstrated. Results are also presented from studies using the EPIC code for several different internal projectile configurations.

15. SUBJECT TERMS
gun charges, solid propellant, multiphase flow, material stress

16. SECURITY CLASSIFICATION OF:			17. LIMITATION OF ABSTRACT	18. NUMBER OF PAGES	19a. NAME OF RESPONSIBLE PERSON
a. REPORT	b. ABSTRACT	c. THIS PAGE			Michael J. Nusca
UNCLASSIFIED	UNCLASSIFIED	UNCLASSIFIED	UL	24	19b. TELEPHONE NUMBER (*Include area code*) 410-278-6108

Standard Form 298 (Rev. 8/98) Prescribed by ANSI Std. Z39.18

Contents

List of Figures

1. Introduction

The interior ballistics environment of the case-telescoped ammunition (CTA) is quite challenging since the gun chamber, normally occupied by the solid propellant charge and a projectile afterbody of small diameter and significant taper, is redesigned so that fully one-quarter of the available chamber volume is occupied by a projectile afterbody of large constant diameter. Concurrently, an acceptable level of projectile muzzle velocity must be maintained so that the propellant loading density of the gun chamber is quite high. Ignition of this tightly-packed charge results in axial pressure waves of such significant amplitude and frequency that the survivability of the projectile must now be called into question. What is needed is an approach that couples the numerical codes used for charge design and the numerical codes that model the structural response of the projectile so that the ammunition designer can arrive at a solution that guarantees the successful launch of a useful payload at a lethal velocity.

Modern interior ballistics (IB) simulation codes are generally capable of modeling the ignition, flamespreading, and combustion of densely-packed advanced charges, even those that include a variety of propellant shapes, such as grains, sticks, disks, and concentric wraps. Most IB codes cannot specifically simulate the CTA configuration since the presence of the projectile afterbody represents both an axially discontinuous and a numerically significant area change in the gun chamber. The U.S. Army's ARL-NGEN3 code is a multidimensional, multiphase computational fluid dynamics (CFD) code (*1–3*). The IB flowfield simulation using this code consists of a discrete component (the propellant) and a continuous component (the gases initially in the chamber and generated by propellant combustion). To capture both types of components, the ARL-NGEN3 code uses a uniquely coupled Eulerian-Lagrangian approach (*1–3*). Previous work has reported the utility of the ARL-NGEN3 code in simulating the CTA configuration (*4*) including the simulation of large amplitude pressure waves around the projectile afterbody and an unsteady pressure loading of the projectile surface.

While IB codes accurately compute the motion of the projectile, they do so while treating it as a rigid body. Such codes cannot model the full response of the projectile to the pressure load imposed on its surface. Vibration and possible damage to or deformation of the projectile are excluded from IB models. These mechanical effects can be simulated using modern computational solid mechanics (CSM) codes, such as DYNA3D (*5*) and EPIC (*6*). DYNA3D and EPIC are both explicit finite-element codes for structural mechanics problems. When the deformation of the projectile is limited to the elastic regime and contact between the projectile and the gun tube occur at relatively low speeds, the accuracy of both the EPIC and DYNA codes on such problems has been demonstrated; therefore, one expects both EPIC and DYNA to give very accurate results in the IB simulation environment.

2. Description of Test Case

There are several goals in the first part of this work; among them is a demonstration of the accuracy, efficiency, and capabilities of the proposed CFD/CSM coupled modeling approach and a determination that the results from DYNA3D and EPIC codes are comparable. To meet these goals, a simplified version of the projectile and charge for a notional large-caliber CTA configuration was defined for this work (*4*, *7–10*). Figure 1 shows the geometry of the projectile afterbody, or tail, and the gun chamber. The chamber is axisymmetric in shape, with no tapering or chambrage, and its diameter and initial length are 14 cm (5.5 in) and 84 cm (33.1 in), respectively. The intruding projectile tail is also axisymmetric in shape, with an outer diameter of 8 cm (3.1 in) and length of 70 cm (27.6 in); the presence of a projectile boattail (i.e., tapered afterbody) and/or aerodynamic fins were excluded for simplicity.

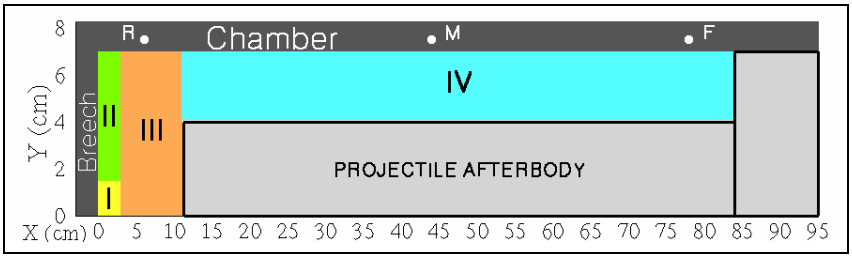

Figure 1. Axisymmetric representation of notional CTA configuration – chamber, projectile afterbody, and four propellant regions shown. Note that region IV fills the annular volume (*4*).

The chamber shown in figure 1 was divided into four regions, each containing a different propellant and/or different propellant geometry. Region I contained 25 g of M1 propellant, which is initially ignited to start the ARL-NGEN3 simulation, and region II contained 25 g of black powder. Regions III and IV were filled with seven-perforated JA2 granular propellant to a loading density of 0.9 g/cm^3.

Figure 2 shows the geometry of the projectiles used in the EPIC and DYNA3D simulations. The codes used slightly different geometries for reasons dealing with the mesh generators used for each of the codes and that will be further discussed later. The sole geometric difference between the two projectiles was that the projectile nosetip was truncated for the projectile used in the DYNA3D simulations. All of the walls of the projectiles were assumed to be 1.25 in (3.175 cm) thick in the first set of simulations. With the EPIC code, a second set of simulations was run in which the walls of the projectile were 0.5 in (1.27 cm) thick. The outer geometry of that projectile was identical to that in the left side of figure 2. The projectiles were assumed to be made of steel; however, the density of the steel was artificially lowered in order to match the 40-lb projectile weight used in the ARL-NGEN3 simulations.

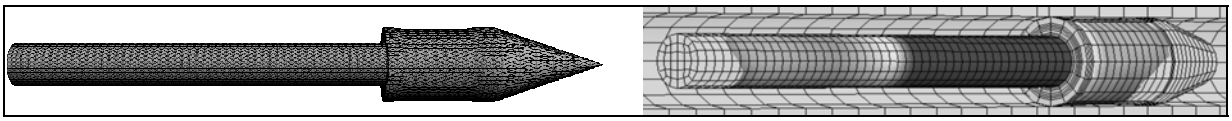

Figure 2. Geometry of the notional CTA projectile and the surface of the mesh used in the EPIC simulation (left) and the DYNA3D simulation (right).

3. ARL-NGEN3 Results

Detailed results from an axisymmetric ARL-NGEN3 simulation of this problem were previously published (*4*, *7–10*). The graph on the left of figure 3 shows the pressure from the ARL-NGEN3 simulation at the points labeled "R," "M," and "F" in figure 1. Notice that there is a pressure spike that occurs at different times for the three axial locations. This is an indication of the strong pressure wave that moves axially through the chamber. The mass of the projectile used in the ARL-NGEN3 simulation was 18.1 kg (weight of 40 lb). Given that weight limit, the pressure load shown in the left half of figure 3 was likely strong enough to damage or destroy a projectile made of any conventional material.

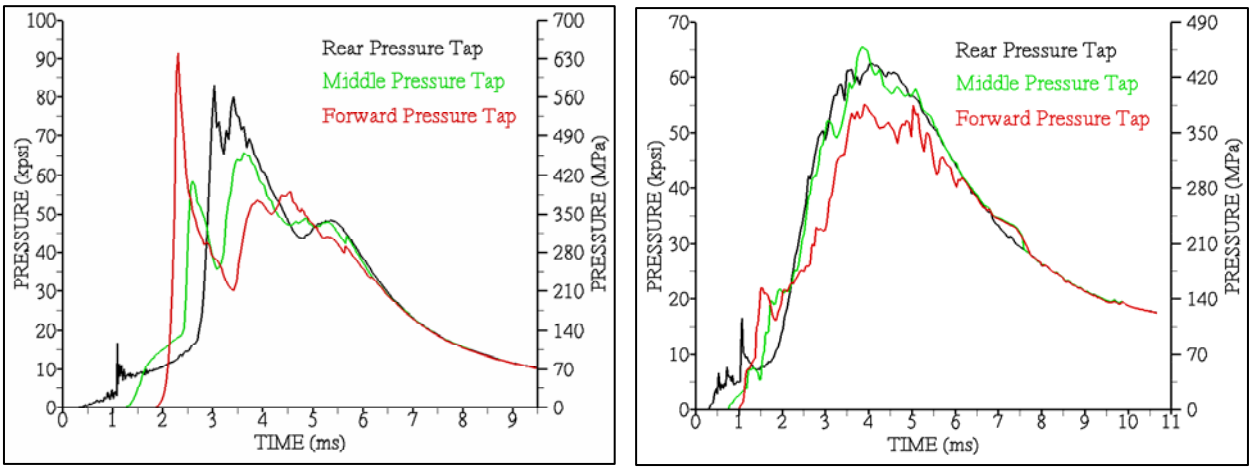

Figure 3. Pressure-time curves predicted using the ARL-NGEN3 code for geometry shown in figure 1 – results for the locations labeled "R," "M," and "F" along the chamber wall: granular propellant (left) and concentric wrap propellant in region IV having minimal axial interphase drag (right). Note that the scales in the right-hand picture are lower than those on the left (*4*, *9*).

The pressure waves seen in the left half of figure 3 arose from several factors, including the high loading density, the geometry of the projectile afterbody, and the resistance to the propellant in region IV (see figure 1) to the axial flow of the high-pressure gas generated during propellant ignition. Another simulation from ARL-NGEN3 explored the effects of the latter factor. In this simulation, the propellant in region IV was assumed to be a concentric wrap propellant with the same thermodynamic characteristics of seven-perforated JA2 granules but with minimal resistance to gas flow in the axial direction (*9*, *10*). The line plot on the right in figure 3 shows

the pressure at three locations in the combustion chamber. The chamber is seen to pressurize more evenly as the pressure waves have been damped significantly. The peak pressure is about one-third less than in the previous case and as a result a projectile made of a conventional material might be able to survive the launch. The drop in muzzle exit velocity, however, is noticeable: 1470 m/s in the former case and 1400 m/s in the latter. Detailed ARL-NGEN3 code results for these simulations, including contour plots of the gas pressure and propellant porosity fields are available in reference (*10*).

4. EPIC/DYNA3D Comparison

In a real gun system any amount of plastic deformation of the projectile is unacceptable. So in the present solid mechanics simulations the projectile material was assumed to respond elastically throughout the gun-firing simulation. The simulations determined if, when, and where the projectile deformed plastically, but they did not predict the effects of such deformation. Limiting the response to the elastic regime simplified the problem, and the results from DYNA3D and EPIC were expected to agree with each other quite well.

The pressure on the surface of the projectile afterbody computed by ARL-NGEN3 was used as input by DYNA3D and EPIC to simulate the mechanical response of the projectile. The geometry of the projectile and the mesh on its surface used in the EPIC and DYNA3D simulations was shown in figure 2. The fine details of the mesh were not expected to affect the computed response in any appreciable way. Mesh generators that came packaged with DYNA3D and with EPIC were used to generate the meshes employed during the respective simulations. Therefore, while the size and number of elements in the two meshes were close, the meshes were not identical. Based on the algorithms used in the EPIC mesh generator, removing the point of the projectile's nose would hurt the time-step size, while in the other mesh generator, including the nose would hurt the time-step size. Provided the mass of the projectiles is equal, the presence or absence of the nose was expected to have very little effect.

A set of simulations was run in order to compare the results from EPIC and DYNA3D; as previously mentioned, the results should agree very well. The 1.25-in wall projectiles were used in these cases. In these simulations, a smaller pressure file from ARL-NGEN3 was used. In order to get this file, the pressure was taken from ARL-NGEN3 every 200 μs, even though pressure data was available roughly every 0.3 μs; the resulting reduced pressure set was referred to as the "sparse" pressure set. Using the sparse pressure set removed a potential source of noise that would make comparisons more difficult. Figure 4 shows the total stress computed by EPIC and by DYNA3D at two points on the projectile tail, one near the back of the projectile forebody, and one roughly halfway along the tail. The DYNA3D results were previously presented (*4*, *8–10*). The meshes used in the simulations were not identical, and so the exact locations where the stress was measured were slightly different in the EPIC simulations versus the DYNA3D

simulations. Nonetheless, the results of the two codes in figure 4 are quite close, agreeing well on the amplitude, frequency, and phase of the oscillations. Figure 5 shows the total stress at 2.4 ms into the gun firing as computed by EPIC and DYNA3D. Again, the agreement between the two solid mechanics codes is very good, even with the slight variation in geometry and mesh. Based on the good agreement and previous validation of the codes, both codes were expected to generate accurate results for this class of problems. The EPIC code was used to generate all of the solid mechanics results presented in the remainder of this report.

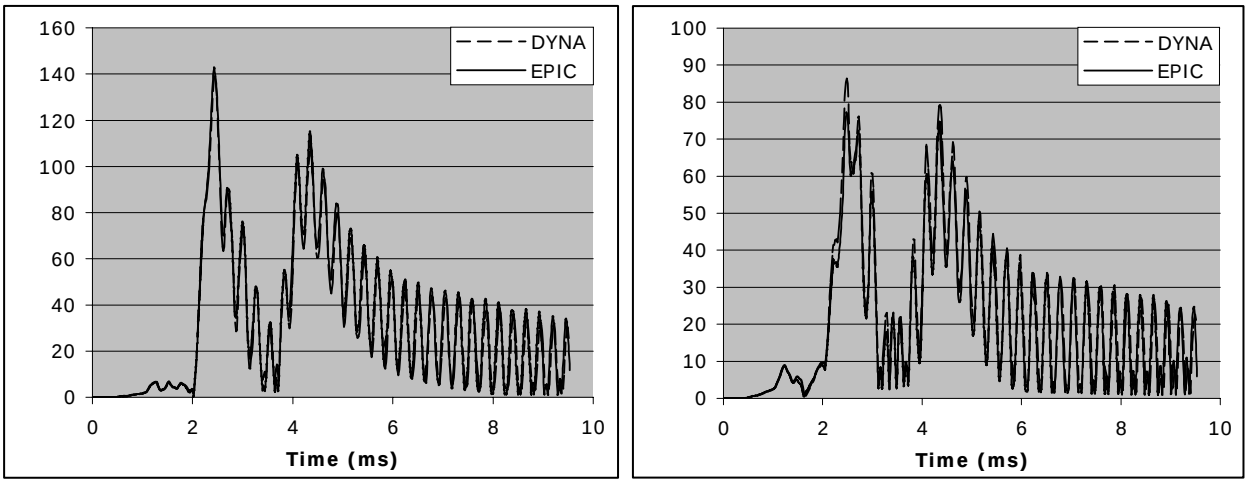

Figure 4. Total stress computed by EPIC (solid line) and DYNA3D (dashed line) near the back of the projectile forebody (left) and near the midpoint of the projectile tail (right).

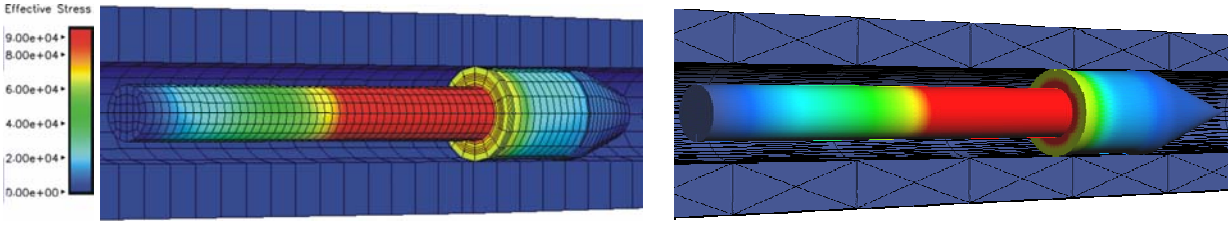

Figure 5. Total stress at 2.4 ms into the gun firing computed by DYNA3D (left) and EPIC (right), near the time of the highest total stress. The red region is where the total stress surpassed 90 ksi (621 MPa); the material likely would have failed and the projectile damaged in that region.

The stresses shown in figure 4 show a strong frequency at about 4 kHz and then after 8 ms another mode starts to be excited with a frequency at about 8 kHz. These are both natural frequencies of the projectile. Recall that the solid mechanics and fluid dynamics solvers are not fully coupled. Therefore, there is neither damping of the solid vibrational modes nor shifting of the projectile's natural frequencies by the gas.

5. Further EPIC Results – 1.25-in Wall Projectile

A simulation was run with EPIC using the full pressure set from ARL-NGEN3. This simulation was run on a SGI Origin 3800 at the U.S. Army Research Laboratory (ARL) Major Shared Resource Center. The full data set was too large for EPIC to read into memory, so the simulation was broken up into several pieces. Figure 6 shows the stress computed at the same locations as in figure 4 using the two data sets. The peak stress is much higher with the full pressure set, and the overall response is more oscillatory.

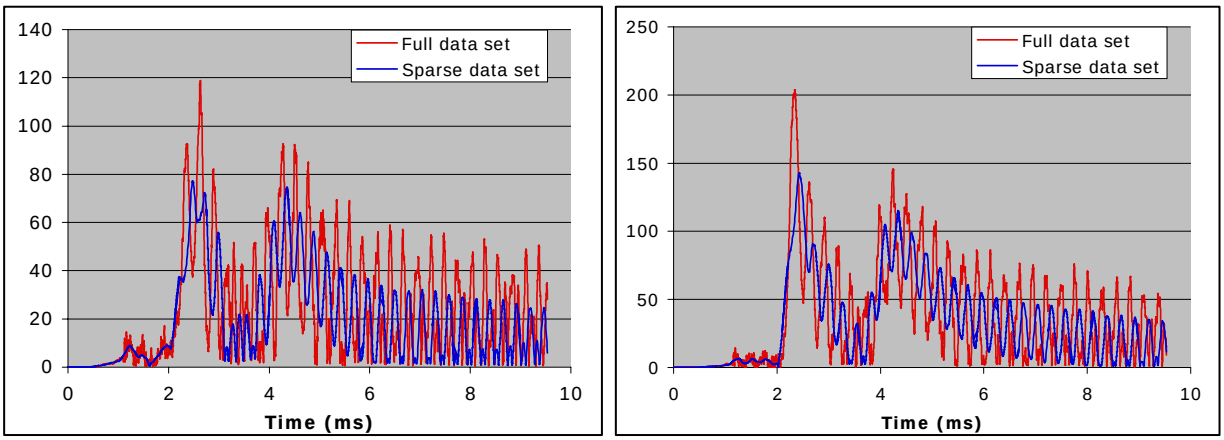

Figure 6. Total stress computed by EPIC using the full data set (red line) and the sparse data set (blue line) near the back of the projectile forebody (left) and near the midpoint of the projectile tail (right).

As mentioned earlier, the full pressure set was too large for the machine being used. So, the pressure was taken from every fourth time level in ARL-NGEN3's data set, and this reduced set was called the "quarter" data set. This data set did fit within the memory of the SGI Origin 3800. Another EPIC simulation used the quarter pressure set, and the results were compared with those that came from the EPIC simulation using the full data set, which are shown in figure 6. The two sets of lines almost perfectly overlaid each other, having no visible differences, so the results are not shown here. All of the rest of the simulations were performed using the quarter set.

A fast Fourier transform of the pressure from ARL-NGEN3 was performed in order to identify the dominant frequencies of the input data. Figure 3 showed line plots demonstrating the trends in the pressure in the gun chamber. The ARL-NGEN3 code uses explicit time-stepping, so the time-step size varied during the simulation, and the code wrote out the pressure at every time step. The pressure was taken every 9.3 μs in order to perform the FFT. The analysis revealed that the pressure data had a strong mode near 100 Hz and progressively weaker oscillations near 500, 1100, and 1700 Hz. The 100-Hz mode was simply the average pressure rise and fall

during the gun firing. The 500-Hz mode was the axially-moving pressure wave that appeared as the double peak in the left half of figure 3.

The frequencies of the computed results from the simulated launch of the 1.25-in-thick wall projectile using the quarter pressure set were determined. As expected, there were very strong signals at 100 and 500 Hz, with slightly weaker signals at 1100 and 1700 Hz. These were the forced modes coming from the pressure computed by ARL-NGEN3. In addition, there was a very strong signal at 3.7 kHz, with other peaks at 3.2, 7.4, 8.5, and 22.8 kHz, as well as other smaller peaks. These frequencies are probably all-natural frequencies of the projectile.

6. Initial Rotation of Projectile

In another simulation, the projectile was initially rotated along the long axis by 1°, i.e., raising the nose while lowering the tail. In order to accommodate this change, the inner and outer diameters of the gun tube were slightly increased. Such changes would be expected to affect the ignition, flamespreading, and combustion during the firing cycle, but that effect was neglected, and the pressure computed by ARL-NGEN3 using the axisymmetric geometry was used in this simulation. Figure 7 shows the total stress at the same two locations in the projectile tail as in figure 6. The projectile began to move about 1.5 ms into the firing cycle, and contact with the chamber wall was first made shortly thereafter. It is interesting to note that, comparing this case with the previous (the axisymmetric projectile placement), the computed stress agreed very well until much later in the firing cycle, about 4.5 ms. After that point, the stress is overall higher in the case with the initially-rotate projectile.

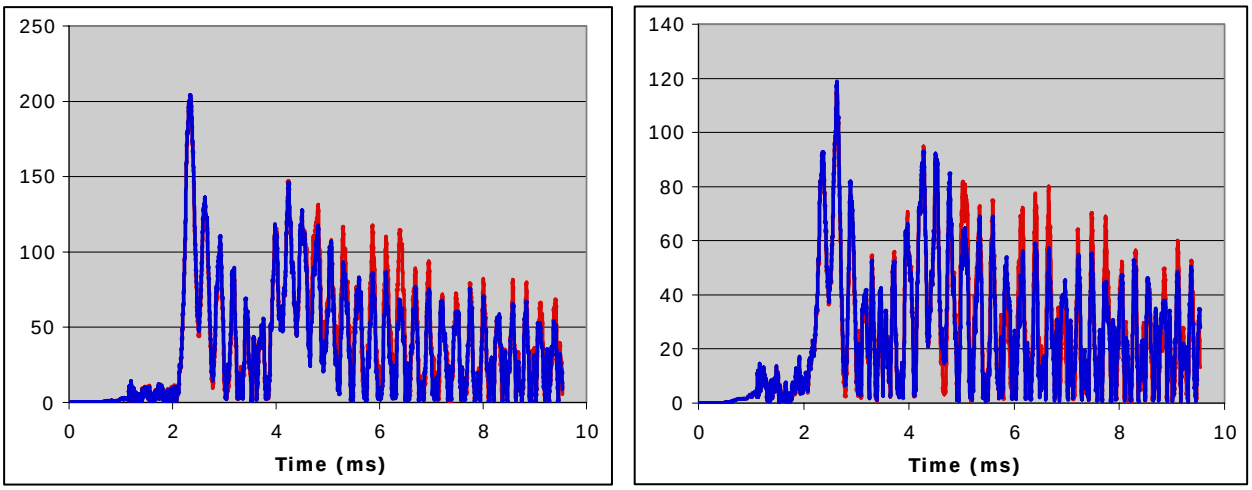

Figure 7. Total stress computed by EPIC for the 1.25-in wall projectile, near the projectile forebody (left) and in the middle of the projectile tail (right). The blue lines show the results from the axisymmetric geometry, and the red lines show the results with the rotated projectile. The stress values did not notably diverge until after 4.5 ms.

7. Propellant With Minimal Interface Drag

A desirable feature of the propellant loaded into region IV (see figure 1) is low interphase drag (resistance to flow) in the axial direction. An ARL-NGEN3 simulation studied the limiting case, in which the granular propellant in region IV had no interphase drag (*9*). The computed pressure looked very similar to that shown in the right half of figure 3, in which, because of the concentric wraps in region IV, there is nearly no axial interphase drag. The launch of the projectile in the initial axisymmetric placement was studied using the pressure results from the no-interphase-drag simulation. Figure 8 shows the total stress from the EPIC simulation along with a repeat of the computed stress from the case first shown in figure 6. The projectile stress for the no-drag propellant does not peak until much later and the maximum is lower than for the real propellant charge. Given the weight limit on the projectile, it would still be a challenge to design a projectile to survive this environment, but it might be possible.

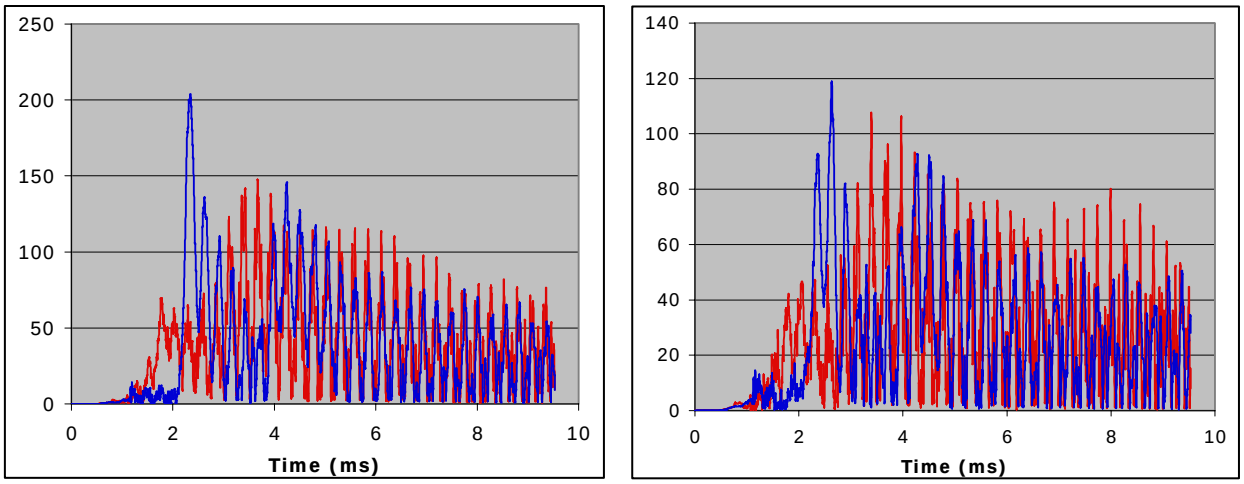

Figure 8. Total stress computed by EPIC for the 1.25-in wall projectile, near the projectile forebody (left) and in the middle of the projectile tail (right) using the pressure in the left half of figure 3 (blue) and from a minimal-interphase-drag ARL-NGEN3 simulation (red). The maximum stress for the latter case is around 150 ksi.

8. The 0.5-in Wall Projectile

A second projectile geometry was used in simulations; in this one, the walls of the projectile are 0.5 in thick. Again, the density of the metal was adjusted so that the mass of the projectile was 18.1 kg. EPIC simulated the launch of this projectile using the quarter pressure set coming from the ARL-NGEN3 simulation involving granular propellant in region IV (shown in the left picture of figure 3). Figure 9 shows the total stress at two points along the projectile tail. The maximum

total stress in this case was much higher than previously, surpassing 350 ksi (2.4 GPa), beyond the yield stress of most metals. The stress was also noisier than in the previous cases. This should all be expected and was caused by the decrease in the wall thickness. Figure 10 shows the total stress in the projectile at 2.4 and 4.4 ms into the simulation. As can be seen in the pictures, it is very unlikely that a projectile made of any conventional metal could have survived the high stresses.

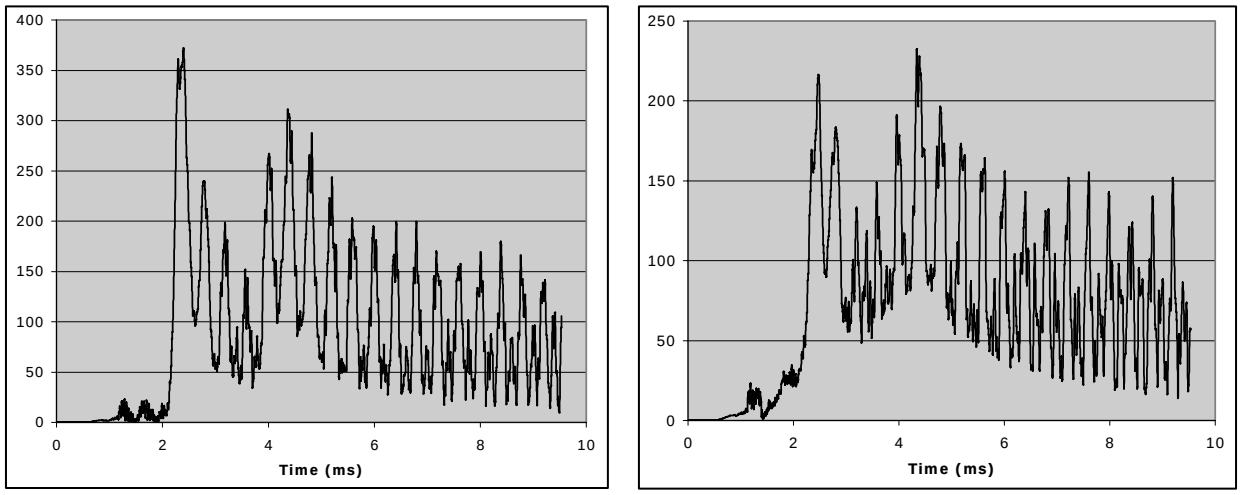

Figure 9. Total stress computed by EPIC for the 0.5-in wall projectile, near the projectile forebody (left) and in the middle of the projectile tail (right). Note the much larger oscillations and higher peak stress compared to figure 6.

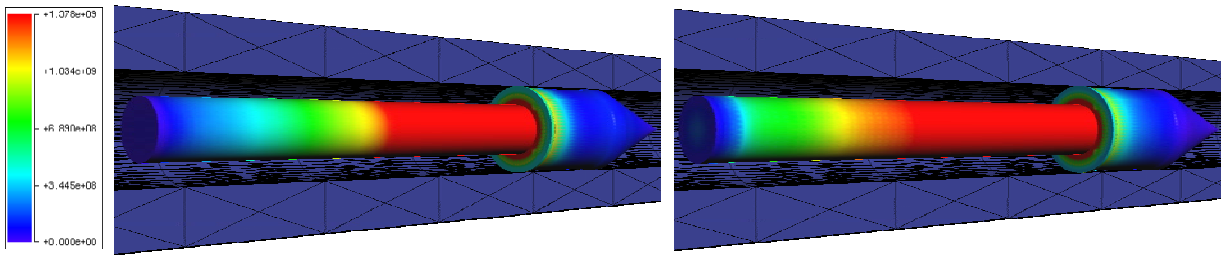

Figure 10. Total stress in the projectile at 2.4 and 4.4 ms into the gun firing. These times correspond to the two peaks in the plots in figure 9. The red regions are where the stress has surpassed 200 ksi (1.38 GPa), so it is very unlikely that any conventional metal could have survived this gun launch.

9. Projectile With Payload

As previously stated, one of the goals of this work is a demonstration of the capabilities of a coupled CFD/CSM approach to studying gun launches. One of the capabilities lays in the study of a payload launched aboard the projectile. The projectiles are hollow and could carry some type of payload, perhaps an explosive or some type of electronics package; the 0.5-in wall projectile especially has a lot of available volume. We know from the work that a 0.5-in wall projectile made of a conventional material probably would not survive the launch. But if the

notional projectile were made of some yet-to-be-determined material that met the weight and strength requirements posed by the pressure load, then the issue becomes what type of loading the payload would experience. To study this, four disks were placed at different locations inside of the projectile. Figure 11 shows the inside of the projectile with the disks. All of the disks were flat circular plates of polycarbonate to represent perhaps a type of electrical component aboard the projectile, and the deformations of the disk were limited to the elastic regime. The foremost disk had a diameter of 10.7 cm (4.2 in) and a thickness of 3.9 cm (1.5 in), and the diameter and thickness of the other disks were 5.2 cm (2.0 in) and 1.3 cm (0.52 in), respectively.

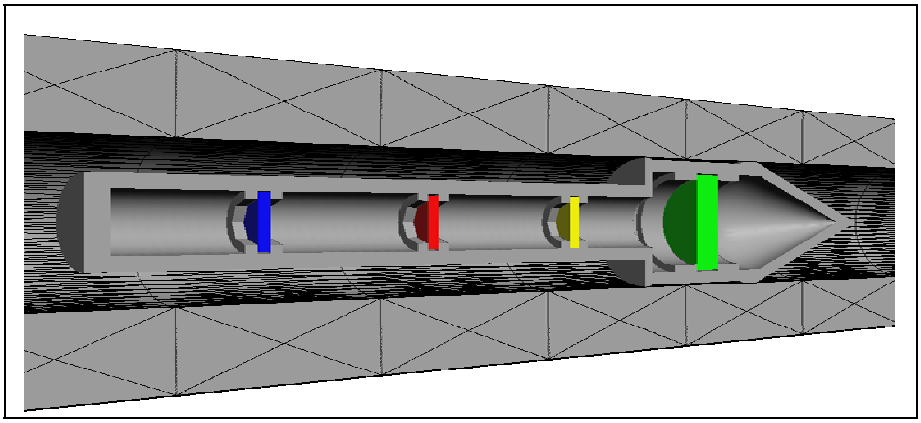

Figure 11. Geometry of the 0.5-in wall projectile carrying four disks; the disk colors correspond to the lines in figure 12. Each disk is held loosely in place by a ridge of steel on either side.

In order to study the survivability of the disks shown in figure 11, it could be important to know the vibrational load and frequencies to which they were subjected. Figure 12 shows the mass-weighted average of the acceleration of the four disks as a function of time. The foremost disk (the green line in figure 12) showed the least oscillations, likely caused by the fact that it was by far the largest of the disks and that the projectile forebody probably vibrated less (in terms of amplitude) than did the projectile tail. The disk midway along the projectile tail (the red line in figure 12) showed the most oscillations. Why that happened has not yet been determined, but it likely was caused by the vibrational modes of the projectile tail that were excited during the gun launch.

In addition to the magnitude of the acceleration, the frequencies at which the disks vibrate could also be important, especially if they were electronic components. All of the signals showed 100-, 500-, and 1100-Hz frequencies, all seen in the pressure input. Above that, the disks vibrated at 2.5, 5.5, 9 (a rather strong signal), and 13 kHz, and at other higher frequencies. Not all of the disks vibrated with every one of these frequencies. There are methods for reducing the vibrational load on the disks, but none were studied in this work. For instance, the disks were allowed to move a little between the steel ridges holding them in place. Other means of securing the disks in place could also have the effect of reducing the vibrational load transmitted to the disks.

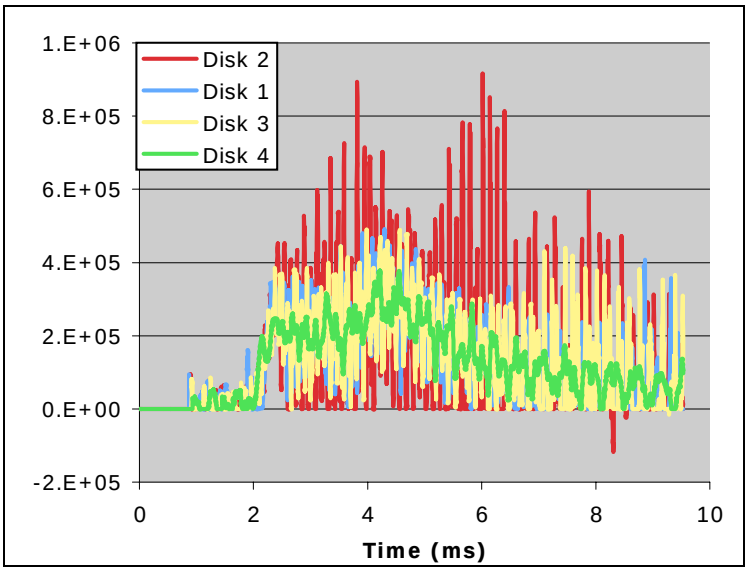

Figure 12. Mass-weighted average of the acceleration of the disks shown in figure 11. The disks are numbered in order with disk 1 on the left (rearmost disk) and disk 4 on the right (foremost disk). The line colors correspond to the disk colors in figure 11.

10. Summary and Conclusions

The interior ballistics environment of the CTA is quite challenging since the gun chamber, normally occupied by the solid propellant charge and a projectile afterbody of small diameter and significant taper, are altered so that fully one-quarter of the available chamber volume is occupied by a projectile afterbody of large constant diameter. Concurrently, an acceptable level of projectile muzzle velocity must be maintained so that the loading density of the gun chamber is quite high. Ignition of this tightly-packed charge results in axial pressure waves of such significant amplitude and frequency that the survivability of the projectile must now be called into question. What is needed is an approach that couples the numerical codes used for charge design (ARL-NGEN3) and the numerical codes that model the structural response of the projectile (DYNA3D and EPIC) so that the ammunition designer can arrive at a solution that guarantees the successful launch of a useful payload at a lethal velocity. The current paper has demonstrated that propellant ignition, flamespreading, and combustion results generated using the ARL-NGEN3 code, can be as successfully linked to the EPIC code as was previously demonstrated for the DYNA3D code. Results from EPIC and DYNA3D, as expected, compared quite well with each other. This modeling effort will continue, with results from ARL-NGEN3 and EPIC being compared with experimental data coming from the work described in (*11*).

11. References

1. Gough, P. S. *Formulation of a Next-Generation Interior Ballistic Code*; ARL-CR-68; U.S. Army Research Laboratory: Aberdeen Proving Ground, MD, September 1993.

2. Nusca, M. J.; Gough, P. S. *Numerical Model of Multiphase Flows Applied to Solid Propellant Combustion in Gun Systems*; AIAA Paper No. 1998-3695, July 1998.

3. Nusca, M. J.; Conroy, P. J. *Multiphase CFD Simulations of Solid Propellant Combustion in Gun Systems*; AIAA Paper No. 2002-1091, January 2002.

4. Nusca, M. J.; Horst, A. W. Progress in Multidimensional, Two-Phase Simulations of Notional Telescoped-Ammunition Propelling Charge. *Proceedings of the 39th JANNAF Combustion Subcommittee Meeting*, Colorado Springs, CO, December 2003; CPIA Publication JSC CD-25.

5. Whirley, R. G.; Engelmann, B. E. *DYNA3D – A Nonlinear, Explicit, Three-Dimensional Finite Element Code for Solid and Structural Mechanics*; UCRL-MA-107254 (Rev. 1); Lawrence Livermore National Laboratory: Oak Ridge, TN, November 1993.

6. Johnson, G. R.; Stryk, R. A.; Holmquist, T. J.; Beissel, S. R. *Numerical Algorithms in a Lagrangian Hydrocode*; WL-TR-1997-7039; Wright Laboratory: Eglin Air Force Base, FL, June 1997.

7. Horst, A. W. Weapon System Constraints on Advances in Gun Propulsion. *Proceedings of the 5th Joint Classified Bombs/Warheads and Ballistics Symposium*, Colorado Springs, CO, 1–2 June 2002.

8. Newill, J. F.; Nusca, M. J.; Horst, A. W. Advances in Coupled Projectile-Dynamics/Interior-Ballistics Simulations: Coupling the DYNA3D Code and the ARL-NGEN3 Code. *Proceedings of the 21st International Symposium on Ballistics*, Adelaide, South Australia, April 2004.

9. Nusca, M. J.; Horst, A. W.; Newill, J. F. Multidimensional, Two-Phase Simulations of Notional Telescoped-Ammunition Propelling Charge. *Proceedings of the 52nd JANNAF Propulsion Meeting*, Las Vegas, NV, May 2004; CPIA Publication JPM CD-04.

10. Nusca, M. J.; Horst, A. W.; Newill, J. F. *Multidimensional, Two-Phase Simulations of Notional Telescoped-Ammunition Propelling Charge*; ARL-TR-3306; U.S. Army Research Laboratory: Aberdeen Proving Ground, MD, September 2004.

11. Williams, A. W.; Colburn, J. W.; Howard, S. L.; Brant, A. L.; Nusca, M. J.; Newill, J. F. Full-Scale Simulator Studies of a Notional Telescoped-Ammunition Charge. *Proceedings of the 40th JANNAF Combustion Subcommittee Meeting*, Charleston, SC, June 2005.

NO. OF
COPIES ORGANIZATION

1 (PDF ONLY) DEFENSE TECHNICAL INFORMATION CTR
DTIC OCA
8725 JOHN J KINGMAN RD
STE 0944
FORT BELVOIR VA 22060-6218

1 US ARMY RSRCH DEV & ENGRG CMD
SYSTEMS OF SYSTEMS INTEGRATION
AMSRD SS T
6000 6TH ST STE 100
FORT BELVOIR VA 22060-5608

1 INST FOR ADVNCD TCHNLGY
THE UNIV OF TEXAS
AT AUSTIN
3925 W BRAKER LN
AUSTIN TX 78759-5316

1 DIRECTOR
US ARMY RESEARCH LAB
IMNE ALC IMS
2800 POWDER MILL RD
ADELPHI MD 20783-1197

3 DIRECTOR
US ARMY RESEARCH LAB
AMSRD ARL CI OK TL
2800 POWDER MILL RD
ADELPHI MD 20783-1197

3 DIRECTOR
US ARMY RESEARCH LAB
AMSRD ARL CS IS T
2800 POWDER MILL RD
ADELPHI MD 20783-1197

ABERDEEN PROVING GROUND

1 DIR USARL
AMSRD ARL CI OK TP (BLDG 4600)

NO. OF COPIES	ORGANIZATION
1	DIR USARL AMSRD ARL D J MILLER 2800 POWDER MILL RD ADELPHI MD 20783-1197
3	DIR USARL AMSRD ARL RO P D MANN R SHAW TECH LIB PO BOX 12211 RESEARCH TRIANGLE PARK NC 27709-2211
8	US ARMY AVIATN & MSLE CMD W CHEW C DOLBEER JS LILLY M LYON JM FISHER BP MARSH RS MICHAELS D THOMPSON REDSTONE ARSENAL AL 35898-5249
2	PM MAS SFAE AMO MAS LTC M BUTLER PICATINNY ARSENAL NJ 07806-5000
2	PM CAS SFAE AMO CAS PICATINNY ARSENAL NJ 07806-5000
7	DIR BENET WEAPONS LAB M AUDINO R DILLON R FISCELLA R HASENBEIN E KATHE K MINER S SOPOK WATERVLIET NY 12189-4050
1	COMMANDER RADFORD ARMY AMMO PLANT SMCAR QA HI LIB RADFORD VA 24141-0298

NO. OF COPIES	ORGANIZATION
18	CDR US ARMY ARDEC D CARLUCCI R CARR R CIRINCIONE S EINSTEIN T GORA J HEDDERICH P HUI J LANNON E LOGSDEN P LU B MACHAK S NICHOLICH P OREILLY J OREILLY J RUTKOWSKI A SABASTO J SHIN R SURAPANENI PICATINNY ARSENAL NJ 07806-5000
1	COMMANDER US ARMY NGIC AMXST MC 3 220 SEVENTH ST NE CHARLOTTESVILLE VA 22901-5396
1	COMMANDANT USAFC&S ATSF CN P GROSS FT SILL OK 73503-5600
2	CDR NAVAL RSRCH LAB TECH LIB J BORIS WASHINGTON DC 20375-5000
1	OFFICE OF NAVAL RSRCH J GOLDWASSER 875 N RANDOLPH ST RM 653 ARLINGTON VA 22203-1927
8	CDR NAVAL SURFACE WARFARE CENTER J CONSAGA R DOHERTY C GOTZMER S MITCHELL S PETERS T C SMITH C WALSH TECH LIB INDIAN HEAD MD 20640-5000

NO. OF COPIES ORGANIZATION

4 CDR
NAVAL SURFACE WARFARE CTR
J FRAYSEE
R FRANCIS
T TSCHIRN
TECH LIB
DAHLGREN VA 22448-5000

3 CDR
NAVAL AIR WARFARE CTR
A ATWOOD
S BLASHILL
T PARR
CH1NA LAKE CA 93555-6001

1 AIR FORCE RESH LAB
MNME EN MAT BR
B WILSON
2306 PERIMETER RD
EGLIN AFB FL 32542-5910

1 AIR FORCE OFC OF SCI RSRCH
M BERMAN
875 N RANDOLPH ST
SUITE 235 RM 3112
ARLINGTON VA 22203-1768

1 NASA LANGLEY RSRCH CTR
D BUSHNELL
MS 110
HAMPTON VA 23681-2199

1 DIR SANDIA NATL LABS
M BAER DEPT 1512
PO BOX 5800
ALBUQUERQUE NM 87185

1 DIR SANDIA NATL LABS
R CARUNG
COMBUSTION RSRCH FACILITY
LIVERMORE CA 94551-0469

2 DIR LAWRENCE LIVERMORE NL
L FRIED
M MURPHY
PO BOX 808
LIVERMORE CA 94550-0622

1 CENTRAL INTELLIGENCE AGNCY
J BACKOFEN
RM 4PO7 NHB
WASHINGTON DC 20505

NO. OF COPIES ORGANIZATION

2 BATTELLE COLUMBUS LAB
TWSTIAC
V LEVIN
505 KING AVE
COLUMBUS OH 43201-2693

1 BATTELLE PNL
M GARNICH
PO BOX 999
RICHLAND WA 99352

1 BATTELLE EAST SCI & TECH
A ELLIS
1204 TECHNOLOGY DR
ABERDEEN MD 21001-1228

2 JHU CHEM PROP INFO AGNCY
W HUFFERD
R FRY
10630 LITTLE PATUXENT PKWY
STE 202
COLUMBIA MD 21044-3200

1 OUSD (AT&L)/STRAT & TACT
SYS MUNITIONS
T MELITA
3090 DEFENSE PENTAGON
RM 3B1060
WASHINGTON DC 20301-3090

1 BRIGHAM YOUNG UNIV
M BECKSTEAD
DEPT OF CHEMICAL ENGRG
PROVO UT 84601

1 CALIF INSTITUTE OF TECHLGY
F E C CULICK
204 KARMAN LAB
MS 301 46
1201 E CALIFORNIA ST
PASADENA CA 91109

2 UNIV OF ILLINOIS
DEPT OF MECH INDUSTRY
ENGINEERING
H KRIER
R BEDDINI
144 MEB 1206 N GREEN ST
URBANA IL 61801-2978

NO. OF COPIES	ORGANIZATION
5	PENNSYLVANIA STATE UNIV DEPT OF MECHANICAL ENGRG K KUO T LITZINGER G SETTLES S THYNELL V YANG UNIVERSITY PARK PA 16802-7501
1	ARROW TECHLGY ASSOC INC 1233 SHELBURNE RD D 8 SOUTH BURLINGTON VT 05403
2	ATK TACTICAL SYSTEMS W B WALKUP T F FARABAUGH 210 STATE RTE 956 ROCKET CENTER WV 26726-3548
1	ALLEGHENY BALLISTICS LAB PO BOX 210 ROCKET CENTER WV 26726
1	ALLIANT TECH SYSTEMS INC C CANDLAND MN07-LW54 5050 LINCOLN DR EDINA MN 55436
3	ATK AMMO & ENERGETICS D A WORRELL W J WORRELL S RITCHIE RADFORD ARMY AMMO PLANT RT 114 PO BOX 1 RADFORD VA 24141-0299
2	ATK THIOKOL P BRAITHWAITE R WARDLE PO BOX 707 BRIGHAM CITY UT 84302-0707
1	ATK ELKTON J HARTWELL PO BOX 241 ELKTON MD 21921-0241

NO. OF COPIES	ORGANIZATION
1	BAE ARMAMENT SYS DIV J DYVIK 4800 E RIVER RD MINNEAPOLIS, MN 55421-1498
2	GEN DYNAMICS ORD/TACT SYS N HYLTON J BUZZETT 10101 DR M L KING ST N ST PETERSBURG FL 33716
3	GENERAL DYNAMICS ST MARKS J DRUMMOND H RAINES D W WORTHINGTON PO BOX 222 SAINT MARKS FL 32355-0222
1	GENERAL DYNAMICS ARM SYS J TALLEY 128 LAKESIDE AVE BURLINGTON VT 05401
1	HICKS AND ASSOCIATES SAIC I MAY 7990 SCIENCE APPLIC CT VIENNA VA 22182
1	PAUL GOUGH ASSOC INC P S GOUGH 1048 SOUTH ST PORTSMOUTH NH 03801-5423
2	VERITAY TECHGY INC R SALIZONI J BARNES 4845 MILLERSPORT HWY EAST AMHERST NY 14501-0305
1	SRI INTERNATIONAL PROPULSION SCIENCES DIV TECH LIB 333 RAVENWOOD AVE MENLO PARK CA 94025-3493
1	SAIC W WAESCHE 1410 SPRING HILL RD SUITE 400 MCLEAN VA 22102

NO. OF
COPIES ORGANIZATION

ABERDEEN PROVING GROUND

1 CDR
USAATC
CSTE DTC AT SL
APG MD 21005

42 DIR USARL
AMSRD ARL WM
W CIEPIELA
AMSRD ARL WM B
J B MORRIS
AMSRD ARL WM BA
D LYON
T KOGLER
AMSRD ARL WM BD
W R ANDERSON
R A BEYER
A L BRANT
S W BUNTE
T P COFFEE
J COLBURN
P J CONROY
B E FORCH
B E HOMAN
AW HORST
S L HOWARD
P J KASTE
A J KOTLAR
C LEVERITT
R LIEB
K L MCNESBY
M MCQUAID
A W MIZIOLEK
J A NEWBERRY
M J NUSCA (6 CPS)
R A PESCE RODRIGUEZ
G P REEVES
B M RICE
R C SAUSA
J SCHMIDT
A W WILLIAMS
AMSRD ARL WM BC
P PLOSTINS
AMSRD ARL WM EG
E SCHMIDT
AMSRD ARL WM M
S MCKNIGHT
AMSRD ARL WM SG
T ROSENBERGER
AMSRD ARL WM T
B BURNS
M ZOLTOSKI

NO. OF
COPIES ORGANIZATION

AMSRD ARL WM TB
P BAKER